Vol 460|30 July 2009|doi:10.1038/nature08207

LETTERS

A viscosity-enhanced mechanism for biogenic ocean mixing

Kakani Katija[1] & John O. Dabiri[1,2]

Recent observations of biologically generated turbulence in the ocean have led to conflicting conclusions regarding the significance of the contribution of animal swimming to ocean mixing. Measurements indicate elevated turbulent dissipation—comparable with levels caused by winds and tides—in the vicinity of large populations of planktonic animals swimming together[1]. However, it has also been noted that elevated turbulent dissipation is by itself insufficient proof of substantial biogenic mixing, because much of the turbulent kinetic energy of small animals is injected below the Ozmidov buoyancy length scale, where it is primarily dissipated as heat by the fluid viscosity before it can affect ocean mixing[2]. Ongoing debate regarding biogenic mixing has focused on comparisons between animal wake turbulence and ocean turbulence[3,4]. Here, we show that a second, previously neglected mechanism of fluid mixing—first described over 50 years ago by Charles Darwin[5]— is the dominant mechanism of mixing by swimming animals. The efficiency of mixing by Darwin's mechanism is dependent on animal shape rather than fluid length scale and, unlike turbulent wake mixing, is enhanced by fluid viscosity. Therefore, it provides a means of biogenic mixing that can be equally effective in small zooplankton and large mammals. A theoretical model for the relative contributions of Darwinian mixing and turbulent wake mixing is created and validated by *in situ* field measurements of swimming jellyfish using a newly developed scuba-based laser velocimetry device[6]. Extrapolation of these results to other animals is straightforward given knowledge of the animal shape and orientation during vertical migration. On the basis of calculations of a broad range of aquatic animal species, we conclude that biogenic mixing via Darwin's mechanism can be a significant contributor to ocean mixing and nutrient transport.

Darwin described a mechanism of fluid mixing by a solid object that does not require the object to generate rotational or shearing motion in the flow[5]. As the solid body travels through fluid, a portion of the surrounding fluid is set into motion by the body's pressure field and propagates along with the body. The volume of fluid that drifts with the solid object is proportional to the volume of the object itself (see Supplementary Fig. 1 and Supplementary Videos 1 and 2). The ratio of drift volume (V_{drift}) to body volume (V_{body})—called the 'added-mass' coefficient—depends only on the shape of the body.

In the case of a vertically stratified fluid such as the ocean, the induced fluid drift caused by vertical motion of a solid body will result in a concomitant change in the total potential energy of the fluid, because higher-density fluid is raised above lower-density fluid during upward body motion (and vice versa during downward body motion). The resulting increased interface between the fluid masses of different density will be susceptible to further stirring by ambient fluid motions and by interaction with neighbouring solid bodies, ultimately leading to molecular mixing[7,8]. The process of potential energy increase via fluid mixing is essential to the maintenance of global ocean circulation and can also facilitate transport of nutrients and other dissolved matter[9]. When the mixing process is entirely fluid-driven, for example, through winds, tides, and potentially the turbulent wakes of swimming animals, the efficiency of the mixing process (that is, the fraction of the fluid kinetic energy that is converted to potential energy) depends on the length scale of the fluid motions. Fluid motions that are smaller than the smallest naturally-occurring ocean length scales (for example, the Kolmogorov and Ozmidov scales) are primarily dissipated as heat by the fluid viscosity and therefore cannot have an impact on ocean mixing[10].

In contrast, Darwin's mechanism of mixing is enhanced by the presence of viscosity in the fluid[11,12]. In the limit of Stokes flow, the induced fluid drift becomes infinitely large[13]. We demonstrated the effect of viscosity by computing the flow around bodies of circular cross-section and diameter D migrating in a viscous fluid at velocity U. The relative effect of viscosity (ν) was manipulated by varying the Reynolds number of the flow, $\mathrm{Re} = UD/\nu$, from 1 to 100. As the drift volume increases monotonically with time in the presence of viscosity[13], we calculated a nominal drift after each body had migrated the same distance. Figure 1a indicates substantial enhancement of the induced drift at decreasing Reynolds numbers. The drift volume in each case is significantly larger than for an equivalent

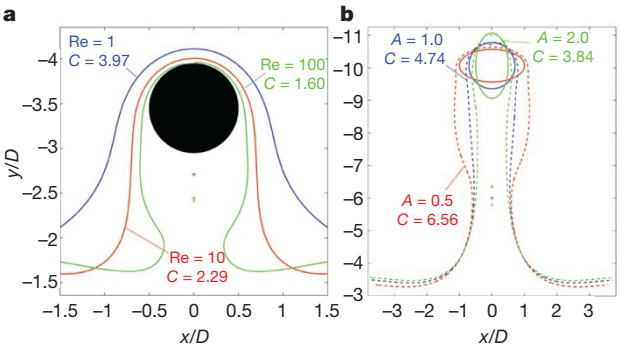

Figure 1 | Numerical simulations of induced vertical drift of initially horizontal layers in the presence of fluid viscosity. a, Simulation of induced fluid drift due to vertical migration of a circular cross-section at Reynolds numbers 1 (blue), 10 (red) and 100 (green). The cylinder moves vertically at unit velocity in each case. The area of induced drift bounded by each curve at the instant shown in the figure and its initial unperturbed horizontal position is indicated in the figure, normalized by the area of the circle (that is, C). Induced drift increases with decreasing Reynolds number. **b**, Simulation of induced fluid drift due to vertical migration of elliptical cross-sections at Reynolds number 10. The fineness (that is, length-to-diameter) ratio A and the normalized drift area C are indicated for each case. Induced drift increases with decreasing fineness ratio. Note that the values of C differ for the circle in panels **a** and **b** because of the difference in time at which the drift area is measured in each case.

[1]Bioengineering, [2]Graduate Aeronautical Laboratories, California Institute of Technology, Pasadena, California 91125, USA.

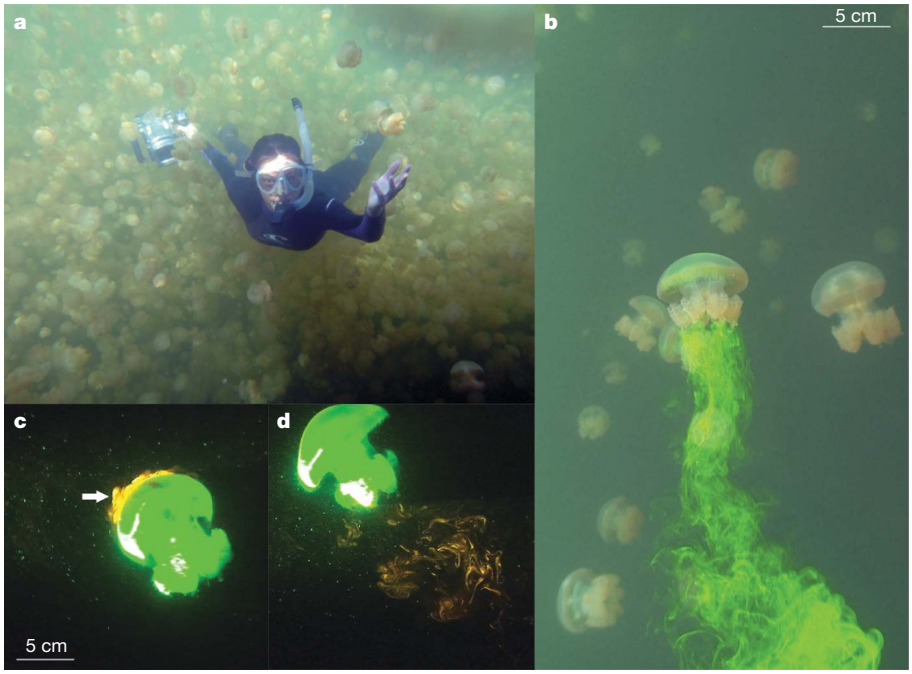

Figure 2 | Field measurements of induced drift during jellyfish swimming. **a**, Image of diver (K.K.) in water column handling the camera for laser velocimetry. (Photo provided by W. M. Graham.) **b**, Induced forward drift of dye behind a swimming *Mastigias* sp. (see also Supplementary Videos 3 and 4). Image is rotated 90°, that is, gravity acts from left to right in the image. **c**, *In situ* measurement of *Mastigias* sp. swimming through an artificially created density stratification (indicated by white arrow). Red fluorescence intensity is proportional to fluid density. **d**, Mixed density field following passage of *Mastigias* sp. The centroid of the density field is shifted in the direction of animal swimming (see Fig. 3). For a vertically migrating animal, this will result in an increase in the potential energy of the fluid. Images are rotated to vertical orientation. See also Supplementary Video 5.

body in an unbounded, inviscid fluid, for which the added-mass coefficient $C = 1$ (ref. 14).

We determined the dependence of Darwin's mechanism on body shape by computing the fluid drift induced by bodies of elliptical cross-section at Re = 10. Figure 1b shows that the drift volume decreases with increasing fineness (that is, length-to-diameter) ratio, consistent with the known trends in inviscid flows. However, the magnitude of the drift induced by even the most prolate body is substantial due to viscous effects at the relatively low Reynolds number.

We experimentally determined the relative contributions of induced drift and wake turbulence to the fluid mixing affected by a swimming animal. *In situ* measurements of swimming jellyfish (*Mastigias* sp., 1–10 cm body diameter) were conducted in a lake in Palau during September 2008 (Fig. 2a). Video recordings of dye injected upstream of individual jellyfish enabled empirical observation of the induced drift effect described above (Fig. 2b; see also Supplementary Videos 3 and 4); dye is carried along behind each animal for several swimming cycles, consistent with the simulations of induced drift above. For quantitative measurements, we constructed a self-contained, underwater velocimetry apparatus[6] to allow a scuba diver to measure directly the wake kinetic energy of freely swimming jellyfish in the water column (see Methods). In addition, planar laser-induced fluorescence measurements of an artificially created stratified layer in mid-water enabled measurement of the change in fluid potential energy caused by a jellyfish swimming through the layer (Figs 2c, d and 3; see also Supplementary Video 5). As the Ozmidov length scale of the injected dye layer ($B \approx 4$ cm) was significantly smaller than the natural buoyancy length scale of the lake[15], the observed dynamics were decoupled from ambient fluid motions. The measurements demonstrated that the mixing process was dominated by the induced drift effects, with 90% of the potential energy increase attributable to induced drift (see Methods). Therefore, neglect of the contribution of induced drift in theoretical models of the mixing efficiency (that is, flux Richardson number) would result in an order-of-magnitude underestimate.

We determined that the contribution of induced fluid drift relative to turbulent wake mixing can be predicted by considering the swimming efficiency of the animal. The Froude propulsive efficiency—the ratio of useable energy for overcoming drag to the total fluid energy input during locomotion—can be approximated as (see Methods)

$$\eta_F \approx \frac{V_{drift}^{2/3} U^3}{V_{drift}^{2/3} U^3 + KN^2 V_{wake} + \left(1 - \frac{V_{drift}^{4/9}}{(\varepsilon/N^3)^{2/3}}\right) \varepsilon V_{wake}} \quad (1)$$

where we have formulated the swimming efficiency in terms of properties of the animal (that is, its swimming speed U and kinetic energy flux per unit time ε into the turbulent wake of volume V_{wake}), the drift volume (V_{drift}), and the ocean (that is, turbulent diffusivity K and Brunt–Väisälä buoyancy frequency

$$N = \sqrt{-g \mathrm{d}\rho / \rho \mathrm{d}z}$$

where g is gravitational acceleration, ρ is the fluid density and z is the vertical coordinate direction). The two terms $KN^2 V_{wake}$ and

$$\left\{1 - \left[V_{drift}^{4/9} \Big/ \left(\varepsilon / N^3\right)^{2/3}\right]\right\} \varepsilon V_{wake}$$

in the denominator of equation (1) together represent the kinetic energy flux per unit time (ε) lost to the turbulent wake as the animal swims; the existing debate over biogenic mixing has focused on their relative magnitudes[1,2]. However, the present simulations and experiments demonstrate that this is only one, potentially small, component of biogenic mixing. Using equation (1) and knowledge of the swimming efficiency, we were able to draw conclusions regarding both the relative contributions of induced drift and turbulent wake mixing in animal swimming, as well as the absolute magnitude of the effect of the Darwinian mechanism on ocean mixing.

Qualitatively speaking, a higher swimming efficiency leads to a larger relative contribution of induced fluid drift to mixing compared with turbulent wake energy. Indeed, in the limit of perfect swimming efficiency, no energy is lost to the wake and Darwin's

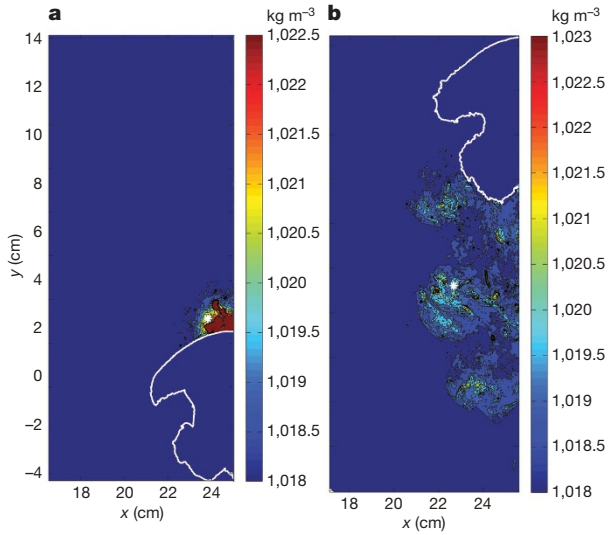

Figure 3 | Analysis of planar laser-induced fluorescence images. **a**, Calibrated density field before passage of *Mastigias* sp. through density stratification. **b**, Calibrated density field following passage of *Mastigias* sp. through density stratification. Change in dye mass centroid is indicated by shift in white dot from panel **a** to panel **b**. Animal position is indicated by white outlines. Images are rotated to vertical orientation.

mechanism is the only one available for fluid mixing. Swimming efficiencies as high as 90% are reported in the literature on aquatic animals[16], consistent with our experimental observations that Darwin's mechanism can dominate over turbulent wake mixing. Even in the limit of low swimming efficiency, Darwin's mechanism will still contribute to mixing because induced drift will persist as long as the animal is moving.

For small animals, that is, those with length scale smaller than the Ozmidov scale B, turbulent mixing becomes inefficient due to the effects of fluid viscosity[2]. In these cases, Darwin's mechanism will be the dominant source of mixing irrespective of the swimming efficiency.

To determine the absolute contribution of Darwin's mechanism to ocean mixing, we note that previous studies of animal wake turbulence estimate kinetic energy production rates on the order of 10^{-5} to 10^{-4} W kg^{-1} for animals spanning a range from 10^{-3} to 10^{1} m in length and 10^{-5} to 10^{3} kg in mass[3]. As the swimming efficiency is of the order 10^{-1} to 1 across the same range of animals[3], we conclude based on equation (1) that the mixing power provided by induced fluid drift is at least of the order 10^{-5} to 10^{-4} W kg^{-1}. This is comparable with the turbulent dissipation observed due to physical processes[1–4] (for example, wind, tides and so on). By a similar argument, the estimated 10^{12} W of total turbulent kinetic energy input per unit time by marine animals[4] indicates that the global contribution to mixing by Darwin's mechanism is also in the range of 10^{12} W. This, too, is of the same order of magnitude as the global contributions of winds and tides. The local contributions of swimming animals to ocean mixing will depend on details of the migration behaviour, which can be heterogeneous even within a single school[17].

We consider these estimates to be conservative because they are based on the fluid transport induced by individual animals swimming in isolation. The drift volumes of neighbouring animals in an aggregation may interact via their boundary layers to enhance vertical transport further, thereby increasing the horizontal scale of the vertically drifting fluid mass to the horizontal extent of the entire aggregation of animals. Furthermore, we have not included in our estimates the effect of passively sinking particulates (for example, marine snow, faecal pellets and so on) that will also induce a drift of the surrounding fluid, with potential implications for downward transport through the deep ocean (for example, carbon sequestration).

METHODS SUMMARY

The online-only Methods detail: (1) analytical and computational modelling of the induced drift effect in inviscid and viscous flows; (2) *in situ* measurement of wake kinetic energy of the swimming animals; (3) measurement of changes in the potential energy of the artificial density stratification due to animal swimming; (4) estimation of the mixing efficiency of a representative animal; (5) estimation of the contribution of induced drift to the change in potential energy; and (6) derivation of equation (1).

Full Methods and any associated references are available in the online version of the paper at www.nature.com/nature.

Received 15 December 2008; accepted 9 June 2009.

1. Kunze, E., Dower, J. F., Beveridge, I., Dewey, R. & Bartlett, K. P. Observations of biologically generated turbulence in a coastal inlet. *Science* **313,** 1768–1770 (2006).
2. Visser, A. W. Biomixing of the oceans? *Science* **316,** 838–839 (2007).
3. Huntley, M. E. & Zhou, M. Influence of animals on turbulence in the sea. *Mar. Ecol. Prog. Ser.* **273,** 65–79 (2004).
4. Dewar, W. K. *et al.* Does the marine biosphere mix the ocean? *J. Mar. Res.* **64,** 541–561 (2006).
5. Darwin, C. Note on hydrodynamics. *Proc. Camb. Phil. Soc. Biol. Sci.* **49,** 342–354 (1953).
6. Katija, K. & Dabiri, J. O. In situ field measurements of aquatic animal-fluid interactions using a self-contained underwater velocimetry apparatus (SCUVA). *Limnol. Oceanogr. Methods* **6,** 162–171 (2008).
7. Eckart, C. An analysis of the stirring and mixing process in incompressible fluids. *J. Mar. Res.* **7,** 265–275 (1948).
8. Eames, I. & Bush, J. W. M. Longitudinal dispersion of bodies fixed in a potential flow. *Proc. R. Soc. Lond. A* **455,** 3665–3686 (1999).
9. Thorpe, S. A. *The Turbulent Ocean* (Cambridge Univ. Press, 2005).
10. Tennekes, H. & Lumley, J. L. *A First Course in Turbulence* (The MIT Press, 1972).
11. Eames, I. The concept of drift and its application to multiphase and multibody problems. *Phil. Trans. R. Soc. Lond. A* **361,** 2951–2965 (2003).
12. Dabiri, J. O. Note on the induced Lagrangian drift and added-mass of a vortex. *J. Fluid Mech.* **547,** 105–113 (2006).
13. Eames, I., Gobby, D. & Dalziel, S. B. Fluid displacement by Stokes flow past a spherical droplet. *J. Fluid Mech.* **485,** 67–85 (2003).
14. Lamb, H. *Hydrodynamics* 6th edn (Cambridge Univ. Press, 1993).
15. Hamner, W. M., Gilmer, R. W. & Hamner, P. P. The physical, chemical, and biological characteristics of a stratified, saline, sulfide lake in Palau. *Limnol. Oceanogr.* **27,** 896–909 (1982).
16. Fish, F. E. Comparative kinematics and hydrodynamics of odontocele cetaceans: morphological and ecological correlates with swimming performance. *J. Exp. Biol.* **201,** 2867–2877 (1998).
17. Parrish, J. K., Viscido, S. V. & Grunbaum, D. Self-organized fish school: an examination of emergent properties. *Biol. Bull.* **202,** 296–305 (2002).
18. Turner, J. S. The flow into an expanding spherical vortex. *J. Fluid Mech.* **18,** 195–208 (1964).
19. Eames, I., Belcher, S. E. & Hunt, J. C. R. Drift, partial drift and Darwin's proposition. *J. Fluid Mech.* **275,** 201–223 (1994).
20. Willert, C. E. & Gharib, M. Digital particle image velocimetry. *Exp. Fluids* **10,** 181–193 (1991).

Supplementary Information is linked to the online version of the paper at www.nature.com/nature.

Acknowledgements We acknowledge W. M. Graham, J. H. Costello and H. Swift for assistance in field measurements and M. Schaadt for preparatory dive assistance. Additional logistical support was provided by the Coral Reef Research Foundation. Field work in Palau was supported by the National Science Foundation Biological Oceanography Program (to M. N. Dawson and J.O.D.). Additional support (to J.O.D.) from NSF Biological Oceanography, Ocean Technology, Fluid Dynamics, and Energy for Sustainability and from the Office of Naval Research (K.-H. Kim) is acknowledged, as are NSF and NDSEG fellowships (to K.K.) and the Charles Lee Powell Foundation.

Author Contributions K.K. and J.O.D. designed the study, analysed the data and wrote the manuscript. K.K. performed the experiments and viscous flow simulations. J.O.D. performed the inviscid flow simulations and derivation of equation (1).

Author Information Reprints and permissions information is available at www.nature.com/reprints. Correspondence and requests for materials should be addressed to J.O.D. (jodabiri@caltech.edu) or K.K. (kakani@caltech.edu).

METHODS

Analytical and computational models. The motion of fluid particles induced by the vertical translation of a sphere was simulated by advecting a horizontal row of particles according to the theoretical solution for the flow around a sphere in inviscid, irrotational flow[18]:

$$v_r = \frac{\mathrm{d}r}{\mathrm{d}t} = -\left(1-\frac{a^3}{r^3}\right)\cos\theta \quad (2)$$

$$v_\theta = r\frac{\mathrm{d}\theta}{\mathrm{d}t} = \left(1+\frac{a^3}{2r^3}\right)\sin\theta \quad (3)$$

where r is the radial coordinate, θ is the angular coordinate measured from the direction of oncoming flow (in the reference frame of the propagating sphere), and a is the sphere radius. Particles in the flow were advected according to the local fluid velocity v, and the drift volume was calculated assuming axisymmetry. The computational domain is 50 sphere radii axially in both directions normal to the reference plane. A partial drift correction[19] was applied to determine the total induced drift volume because the radial extent of the horizontal row tracked in the simulation was finite.

The motion of fluid particles induced by the passage of two-dimensional bodies of circular and elliptical cross-section through viscous flow at Re = 1, 10 and 100 was computed using the Fluidica software tool (T. Colonius and K. Taira, California Institute of Technology).

Wake kinetic energy measurement. Velocity fields were measured using digital particle image velocimetry[6,20]. The scuba diver operating the system remained motionless in the water column as animals swam freely into the plane of a 1-mm thick vertical sheet of light produced by a 250 mW, 532 nm diode-pumped solid-state laser (Wicked Lasers). The laser sheet illuminated natural particulates in the sea water (typically 10–100 μm), and the particle motion induced by the animal swimming was recorded at 30 Hz using a high-definition (1,920 × 1,080 pixels) complementary metal-oxide–semiconductor camera (Sony). Consecutive images of each video were interrogated with a digital particle image velocimetry algorithm, using an interrogation window size of 64 × 64 pixels and 50% window overlap. A representative case of swimming was selected for in-depth analysis of the wake kinetic energy.

The wake kinetic energy was computed at each node i of the velocity field according to the definition $KE_i = \frac{1}{2}\rho\forall_i\|\mathbf{u}_i\|^2$, where ρ is the ambient water density (1,020 kg m^{-3}), $\forall_i$ is the volume of the node (assuming radial symmetry about the animal body axis), and $\|\mathbf{u}_i\|$ is the magnitude of the velocity (that is, the speed) at each node. The total wake kinetic energy was determined by summing the energy at each of the nodes in the wake. The maximum increase in wake kinetic energy during each swimming cycle, ΔKE, was identified from the temporal trend of the wake kinetic energy measurements. The corresponding dissipation rate ε was estimated as $\Delta KE/mT_c$ where m is the mass of fluid encountered by the animal per swimming cycle and T_c is the duration of bell contraction.

Potential energy and mixing efficiency measurement. A sheet of fluorescent dye mixture of known density, ρ_{dye} (<1% above ambient $\rho_{ambient}$), was injected upstream of swimming *Mastigias* sp. and recorded using the optics described in the previous section. Fluorescence intensity was correlated with fluid density via an a priori laboratory calibration. The displacement, Δh, of the dye centroid along the direction of animal swimming (not necessarily vertical) was measured using an in-house image processing code and was used to infer the change in fluid potential energy for a vertically migrating animal as $\Delta PE = (\rho_{dye} - \rho_{ambient})V_{dye}g\Delta h$, where V_{dye} is the volume of injected dye. The total mixing efficiency (that is, flux Richardson number) was given by the ratio $\Delta PE/\Delta KE$ and was 24 ± 18% for a representative measurement, with the primary source of measurement uncertainty being the value of V_{dye} estimated from the dye images. The corresponding Brunt–Väisälä buoyancy frequency was computed according to the definition

$$N = \sqrt{-g\mathrm{d}\rho/\rho\mathrm{d}z},$$

where dz was estimated based on the length scale of the dye patch before interaction with the animal (≈2 cm). The corresponding Ozmidov buoyancy length scale was computed according to the definition $B = \sqrt{\varepsilon/N^3}$ and was nominally 4 cm.

Induced drift estimation. As the shape of the induced drift region is approximately conical during the first few body lengths of travel through the stratified layer[11], the contribution of induced drift to the measured fluid displacement Δh was estimated based on the distance from the base to the centroid of a right circular cone with base and slant height equal to the characteristic length, L, of the animal. Hence, the contribution from induced drift to the measured change in dye centroid, Δh_{drift}, was estimated as $\sqrt{3/64}L$. For the Mastigias measurement, $\Delta h_{drift}/\Delta h \approx 0.9$, indicating a dominant contribution of induced drift to the change in fluid potential energy.

Froude efficiency derivation. The Froude propulsive efficiency is defined as the ratio of useful work to the total input of energy during swimming, and can be written as

$$\eta_F = \frac{F_D U}{F_D U + \varepsilon} \quad (4)$$

where F_D is the drag force on the animal, U is the swimming speed, and ε is the flux of kinetic energy into the wake per unit time. As an order-of-magnitude estimate, the drag per unit fluid density can be approximated as $F_D \approx V_{drift}^{2/3}U^2$, where for the sake of convenience in what follows, the characteristic area over which hydrodynamic forces act is derived from the drift volume, that is, $V_{drift}^{2/3}$. The wake energy flux per unit time ε can be partitioned[2] into the portion that contributes to changes in the potential energy of the fluid, KN^2 and the portion that is dissipated as heat by the fluid viscosity, $(1-\Gamma_\varepsilon)\varepsilon$, which depends on the mixing efficiency Γ_ε. For animals smaller than the characteristic buoyancy length scale of the stratified fluid, the mixing efficiency can be estimated[2] as

$$\Gamma_\varepsilon \approx \left[V_{drift}^{1/3}\Big/\left(\varepsilon/N^3\right)^{1/2}\right]^{4/3},$$

where the characteristic length scale of the body is again derived from its drift volume, that is, $V_{drift}^{1/3}$. Substituting these expressions into equation (4), we arrived at the relationship given in equation (1).